fluids[35]. Perhaps Ni is precipitated at depth instead of being added to the hydrothermal system. Whether metal-rich magmatic fluids may be transferred to a hydrothermal system remains unresolved; the possible mechanism of such a process is also unclear. □

Received 10 April; accepted 14 August 1996.

1. Lydon, J. L. *Geosci. Can.* **15,** 43–65 (1988).
2. von Damm, K. L. *Annu. Rev. Earth Planet. Sci.* **18,** 173–204 (1990).
3. Cathles, L. M. *Econ. Geol.* **88,** 1977–1988 (1993).
4. Stanton, R. L. *Ore Elements in Arc Lavas* (Clarendon, Oxford, 1994).
5. Fenner, C. N. *Ore Deposits of the Western States (Lindren Vol.)* Ch.III, Pt 1, 58–106 (Am. Inst. Mining & Metallurgical Engrs, New York, 1933).
6. Urabe, T. & Marumo, K. *Episodes* **14,** 246–251 (1991).
7. De Ronde, C. E. J. in *Magmas, Fluids, and Ore Deposits* (ed. Thompson, J. F. H.) 479–510 (Mineralogical Assoc. of Canada, Ottowa, 1995).
8. Franklin, J. M., Lydon, J. W. & Sangster, D. F. *Econ. Geol.* (75th Anniv. Vol.) 485–627 (1981).
9. Hedenquist, J. W. & Lowenstern, J. B. *Nature* **370,** 519–527 (1994).
10. Scott, S. D. *Mar. Min.* **5,** 191–212 (1985).
11. Rona, P. A. & Scott, S. D. *Econ. Geol.* **88,** 1933–1976 (1993).
12. Roedder, E. *Fluid Inclusions* (Mineralogical Soc. Am., Washington DC, 1984).
13. Cashman, K. V. & Mangan, M. T. in *Volatiles in Magmas* (eds Carroll, M. R. & Holloway, J. R.) 447–478 (Mineralogical Soc. Am., Washington DC, 1994).
14. Taylor, B., Crook, K. A. W., Sinton, J. M. & Petersen, L. in *Pacific Sea Floor Atlas* Sheets 1–7 (Hawaii Inst. of Geophys, Honolulu, 1991).
15. Binns, R. A. & Scott, S. D. *Econ. Geol.* **88,** 2226–2237 (1993).
16. Scott, S. D. & Binns, R. A. in *Hydrothermal Vents and Processes* (eds Walker, L. M. & Dixon, D. R.) 191–205 (Spec. Publ. No. 87, Geol. Soc., London, 1995).
17. Javoy, M. & Pineau, F. *Earth Planet. Sci. Lett.* **107,** 598–611 (1991).
18. Kelley, D. S. *J. Geophys. Res.* **101,** 2943–2962 (1996).
19. Gerlach, T. M. & Graeber, E. J. *Nature* **313,** 273–277 (1985).
20. Mathez, E. A. in *Ore Deposition Associated with Magmas* (eds Whitney, J. A. & Naldrett, A. J.) 21–32 (Rev. Econ. Geol. 4, Soc. of Economic Geologists, Littleton, Colorado, 1989).
21. Dixon, J. E. & Stolper, E. M. *J. Petrol.* **36,** 1633–1646 (1995).
22. Lowenstern, J. B., Mahood, G. A., Rivers, M. L. & Sutton, S. R. *Science* **252,** 1405–1409 (1991).
23. Lowenstern, J. B. *Contr. Mineral. Petrol.* **114,** 409–421 (1993).
24. Heinrich, C. A., Ryan, C. G., Mernagh, T. P. & Eadington, P. J. *Econ. Geol.* **87,** 1566–1583 (1992).
25. Ballhaus, C., Ryan, C. G., Mernagh, T. P. & Green, D. H. *Geochim. Cosmochim. Acta* **58,** 811–826 (1994).
26. Fleet, M. E. & Wu, T. *Geochim. Cosmochim. Acta* **59,** 487–495 (1995).
27. Stoiber, R. E. & Rose, W. I. Jr *Geochim. Cosmochim. Acta* **38,** 495–516 (1974).
28. Joran, Y. A., Hedenquist, J. W., Korzhinsky, M. A., Tkachenko, S. I. & Shmulovich, K. *Geochim. Cosmochim. Acta* **59,** 1749–1761 (1995).
29. Sakai, H. *et al. Science* **248,** 1093–1096 (1990).
30. Urabe, T. *et al. Science* **269,** 1092–1095 (1995).
31. Jaupart, C. & Tait, S. in *Modern Methods of Igneous Petrology: Understanding Magmatic Processes* (eds Nicholls, J. & Russell, J. K.) 213–238 (Mineralogical Soc. Am., Washington DC, 1990).
32. Ernst, W. G. *Petrologic Phase Equilibrium* 333 (Freeman, San Francisco, 1976).
33. Peacock, S. M. *Science* **248,** 329–337 (1990).
34. Urabe, T. *Econ. Geol.* **82,** 1049–1052 (1987).
35. von Damm, K. L. *et al. Geochim. Cosmochim. Acta* **49,** 2197–2220 (1985).
36. Weast, R. C. & Astle, M. J. *CRC Handbook of Chemistry and Physics* B-98 (CRC, Boca Raton, 1982).
37. Moore, J. M. & Calk, L. *Am. Mineral.* **56,** 476–488 (1971).

ACKNOWLEDGEMENTS. We thank C. de Ronde and J. Lowenstern for their comments. This work was supported by the Natural Sciences and Engineering Research Council of Canada, and the Bank of Nova Scotia (S.D.S.) and an NSERC International Fellowship (K.Y.)

CORRESPONDENCE should be addressed to S.D.S. (e-mail: scottsd@ecf.utoronto.ca).

An abiotic model for stromatolite morphogenesis

John P. Grotzinger & Daniel H. Rothman

Department of Earth, Atmospheric and Planetary Sciences, Massachusetts Institute of Technology, Cambridge, Massachusetts 02139, USA

STROMATOLITES are laminated, accretionary structures, which are commonly regarded to have formed by the sediment-binding or precipitating activities of ancient microbial mats or biofilms (composed mainly of cyanobacteria), possibly supplemented by abiotic surface precipitation[1–4]. Stromatolites are thus considered to be a proxy for early life on Earth, as the record of these structures extends back to 3.5 Gyr ago[5]. But as stromatolites only rarely contain fossil microbes, their biogenicity is tacitly assumed on the basis of morphological comparisons with modern, demonstrably biological, structures[6]. Little is known about the physical, chemical and biological processes that controlled the growth of ancient stromatolites[4] and, with pioneering exceptions[7–9], the analysis of the inherent geometric characteristics of the structures has not been pursued. Here we present a morphological characterization of ancient stromatolites that have growth surfaces with self-affine fractal geometry. We deduce, from both the microscopic textures and the fractal dimension, a purely abiotic dynamical model of stromatolite surface growth that combines chemical precipitation on the growing interface, fallout and diffusive rearrangement of suspended sediment, and uncorrelated random noise. This result calls into question the assumption that organisms—even if present—necessarily played an essential role in determining stromatolite morphology during times when precipitation at the sea floor was common, such as the earlier Precambrian.

The stromatolites analysed in this study form part of a 1.9-Gyr-old subtidal reef developed within the foreland basin of Wopmay orogen, northwestern Canada[10,11]. The reef is part of the shallowing-upward Cowles Lake Formation in which deep basinal limestone rhythmites and siliciclastic turbidites are overlain by prograding slope facies, capped by reef and back-reef intraclast/ooid grainstone. The reef is 20 metres thick and primarily consists of peak-shaped stromatolites, although domal stromatolites also are locally abundant[11]. Stromatolite growth surfaces are expressed as laminae which are remarkably irregular, forming a hierarchy of peaks of differing size, and separated by U-shaped depressions (Fig. 1). A high degree of surface roughness is expressed across many different length scales. Three different lamina types are present: (1) laminae, often dark, that preferentially thicken into the depressions; (2) lighter laminae that are uniformly thick in the direction normal to the growth surface; and (3) light laminae that form millimetre-scale irregular projections (Fig. 1*a*). All laminae consist of fine, microsparitic calcite, with crystal sizes generally in the range of 5–10 μm; darker laminae may contain several per cent clay and silt-sized siliciclastic detritus.

Photographs were taken of the peak-shaped stromatolites exposed along outcrop faces oriented normal to the growth direction (Fig. 1*b*), and representative samples were collected, cut normal to the growth direction, and polished (Fig. 1*a*) for detailed analysis. Stromatolitic growth laminae revealed in the polished slab and in the field photograph were traced and digitized for values of height h_j at horizontal locations x_j, $j = 1, \ldots, N$, at uniform intervals Δx. If the lamina failed to be single-valued at some x_j, then the average height of that lamina at that x_j was chosen instead. Eleven growth laminae of horizontal length $L = 0.065$ m were obtained (with $N = 64$ and $\Delta x = 1.0$ mm) from the polished slab. Seventeen growth laminae of length $L = 1.20$ m (with $N = 128$ and $\Delta x = 9.4$ mm) were obtained from the field photograph of the outcrop. Each digitized lamina then was multiplied by a Hanning (cosine taper) window function[12] and its power spectrum

$$S(k) = \frac{L}{2\pi}\left|\frac{1}{N}\sum_{j=0}^{N=1} h_j e^{i2\pi jk/N}\right|^2, \quad k = 0, \ldots, N-1 \qquad (1)$$

was calculated. The average power spectra $\langle S(k)\rangle$ for the polished slab and field photograph, respectively, are shown in Fig. 2. Without adjusting any prefactors, both power spectra obey the same power law $\langle S(k)\rangle = Ak^{-\beta}$, where A is a constant and the exponent $\beta = 2.01 \pm 0.03$ was obtained from linear regression. The two power spectra collectively span nearly three orders of magnitude in wavenumber, with wavelengths ranging from 0.002 to 1.2 m.

The power-law decay of $\langle S(k)\rangle$ shows that the stromatolite laminae have self-affine fractal geometry, where the fractal dimension D may be obtained[13] from the relation $D = 1 + (5 - \beta)/2$. We thus find $D = 2.50 \pm 0.02$. Having found this one-parameter characterization of stromatolite morphology, we wish to use it to deduce the dynamics of stromatolite growth.

We propose the following mechanisms for the growth of stromatolites in general, for which our example is a particular

case. These mechanisms are: (1) fallout of suspended sediment; (2) diffusive smoothing of the settled sediment (that is, sediment moves downhill at a rate proportional to slope) and surface tension effects in chemical precipitation; (3) surface-normal precipitation; and (4) uncorrelated random noise representative of surface heterogeneity and environmental fluctuations. Viewing these processes macroscopically, that is, in terms of a continuum partial-differential equation, we may express these growth mechanisms as

$$\frac{\partial h}{\partial t} = v_s + \kappa\nabla^2 h + v_p\sqrt{1+(\nabla h)^2} + \eta(x,t) \qquad (2)$$

where the four terms on the right-hand side correspond specifically to the four mechanisms listed above, respectively. Thus v_s is the time-averaged rate of upward growth through sediment settling, κ is an effective diffusion coefficient, v_p is the time-averaged rate of surface-normal precipitation, and η is uncorrelated random noise with zero mean and variance η_0^2. The square-root factor is a geometric correction that acts to project the surface-normal growth along the h-axis. The smoothing represented by the second term of equation (2) is equally representative of surface tension and diffusion. The net effect of these two processes is combined into the single coefficient κ. In the case of our stromatolite in particular, and other stromatolites in general (including convex-upward morphotypes), the effects of surface tension will tend to dominate in laminae formed by precipitation (the light layers in Fig. 1) whereas the effects of diffusion will tend to dominate in layers which have formed by the fallout of suspended sediment (the dark laminae in Fig. 1).

Assuming that $|\nabla h| \ll 1$, we approximate it by $1 + 0.5(\nabla h)^2$. Then, transforming equation (2) to the comoving frame $h' = h - (v_s + v_p)t$ and dropping primes, we obtain the interface evolution equation of Kardar, Parisi and Zhang[14]:

$$\frac{\partial h}{\partial t} = \kappa\nabla^2 h + \frac{v_p}{2}(\nabla h)^2 + \eta(x,t) \qquad (3)$$

Numerical solutions of equation (3) and related models for which the contribution from surface-normal growth is not small (specifically, when the quantity $\varepsilon = v_p\eta_0/\kappa^3$ is not insignificant) yield interfaces that evolve to a statistical steady state with fractal dimension $D \approx 2.6$ independent of initial conditions[15–17]. Assuming that our measurement of $D \approx 2.5$ is not significantly different from the theoretical prediction of $D \approx 2.6$, our theoretical description is consistent with our quantitative measurements.

We note that when $\varepsilon \to 0$ (that is, when the contribution from the nonlinearity in equation (3) is insignificant), equation (3) predicts $D = 3$ (ref. 18), in clear contradiction to our measurements. Thus the inclusion of surface-normal precipitation in our mechanistic theory appears essential. Surface-normal growth in the case of the stromatolite studied here involves the precipitation of the two, generally lighter types of laminae (Fig. 1*a*): one which maintains constant thickness independent of local slope, and another which is expressed by growth of irregular projections that generally are covered by the darker sediment. Some of the taller projections, however, are incompletely covered and influence the shape of overlying laminae, resulting in sharp peaks separated by concave-upward depressions. The irregular projections, which occur at a scale smaller than our resolution but which microscopically show no evidence for preservation of filament moulds or other biogenic microtextures, influenced the structure of the stromatolite reef over a broad range of length scales to generate its characteristic peaked structure. Thus they constitute the building blocks of an iterative process. Although most other stromatolites produce convex-upward, dome-shaped laminae, our four generic growth mechanisms should still be present. Although our theoretical description has been justified by the use of only one parameter—the fractal dimension D—we note that further confirmation could come from measurement of the time-dependent roughening of initially flat surfaces[14]. Thus, future studies should concentrate on the surfaces upon which stromatolite growth is initiated and the way that lamina shape changes upward.

We note that the mechanisms invoked in equation (3) are derived from examination of the stromatolite itself and the quantitative measurement of our stromatolite approximately fits the prediction of a theory. Significantly, the deterministic form of equation (3) describes the evolution of interfaces which are qualitatively similar to growth forms of many stromatolites with more typical, convex-upward morphology (see Fig. 1 of ref. 14 and compare with the image on page 8 of ref. 3). Thus, we consider that we have developed a model which not only approximately fits a measured exponent, but also conforms to physically plausible mechanisms derived from the observations of the stromatolite growth textures themselves.

Our result demonstrates that the morphology of at least some, and perhaps many, types of stromatolites may be accounted for exclusively by abiotic mechanisms, particularly where growth by precipitation is thought to be important. However, insomuch as microorganisms exist in virtually all shallow marine environments

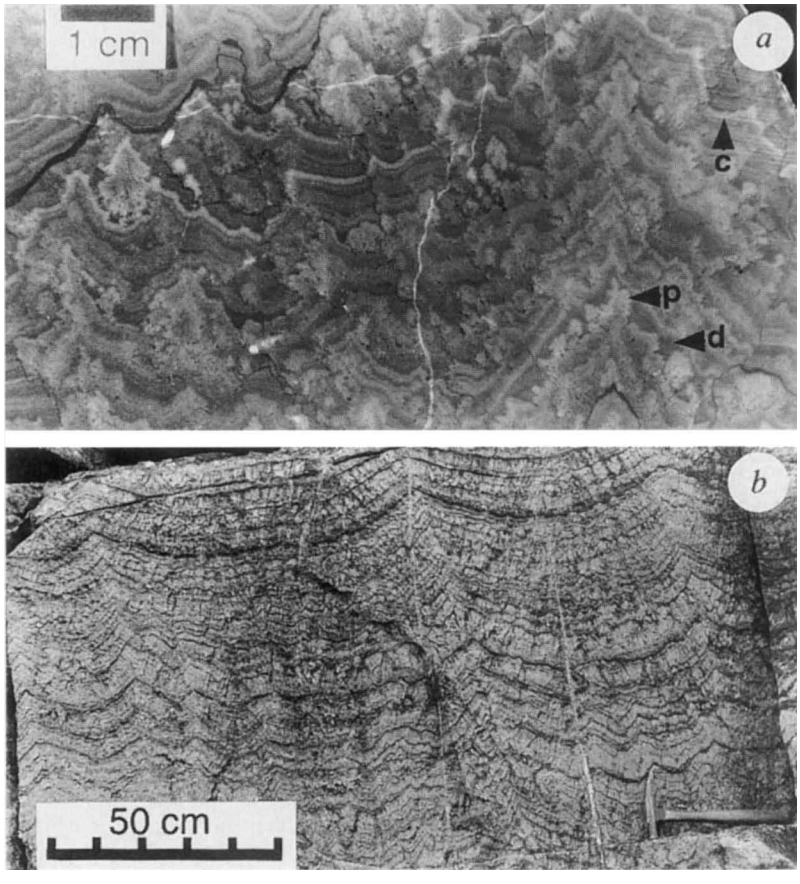

FIG. 1 Peaked-shaped stromatolites from the Cowles Lake Formation reef complex. *a*, Polished slab. Stromatolitic lamination is represented by three types (arrowed) which: thicken into depressions and tend to be darker coloured (d); form lighter layers of constant thickness as measured normal to the growth surface (c); form lighter layers with millimetre-scale, irregular projections that grow normal to the growth surface (p). Note that the millimetre-scale irregular projections are the source of the peaked structure at all larger scales. *b*, Outcrop photograph showing peaks at intermediate and largest scales.

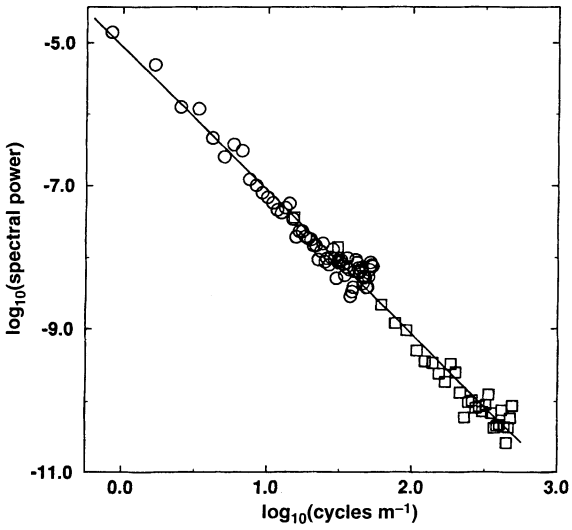

FIG. 2 Plot of $\log_{10}S(k)$ versus $\log_{10}k$, for both the field photograph (circles) and polished slab (squares), compared to the best-fitting line from linear regression (straight line). Both sets of data fit the relation $S(k) \approx k^{-\beta}$ where $\beta = 2.01 \pm 0.03$. The power-law decay of $S(k)$ shows that no single wavenumber component dominates the power spectrum and that the geometry of the stromatolite laminae is statistically scale invariant.

today, it would be misleading to assume that they did not inhabit the surfaces of most, if not all, Precambrian stromatolites. But if they did, then it is no longer clear what role they played in morphogenesis. As the textural evidence for precipitation in stromatolite growth continues to increase[19–23], particularly for early Precambrian time when stromatolites are regarded as an important proxy for life on Earth it seems prudent to remain cautious in the assumption of biogenicity without direct evidence supplied by the presence of fossilized microbes that can be shown to have influenced morphogenesis (that is, were not passively residing on a convenient substrate). In attempting to demonstrate through rigorous analysis that morphology may uniquely reflect biology, we emphasize that the null hypothesis—that morphology is the result of physical and chemical processes—cannot be falsified in the case studied here and probably for many other stromatolites. □

Received 29 December 1995; accepted 9 August 1996.

1. Kalkowsky, V. H. E. *Z. Deutsch. Geolosischen Gesellschaft* **60,** 68–125 (1908).
2. Young, R. B. *Trans. Proc. Geol. Soc. S. Africa* **35,** 29–36 (1932).
3. Walter, M. R. (ed.) *Stromatolites* (Elsevier, Amsterdam, 1976).
4. Ginsburg, R. N. in *Controversies in Modern Geology* 25–36 (Academic, London, 1991).
5. Schopf, J. W. *Earth's Earliest Biosphere* (Princeton Univ. Press, 1983).
6. Buick, R., Dunlop, J. S. R. & Groves, D. I. *Alcheringa* **21,** 161–181 (1981).
7. Hofmann, H. J. in *Stromatolites* (ed. Walter, M. R.) 45–54 (Elsevier, Amsterdam, 1976).
8. Zhang, Y. & Hofmann, H. J. *J. Geol.* **90,** 253–268 (1982).
9. Hofmann, H. J. *J. Paleontol.* **68,** 704–709 (1994).
10. Hoffman, P. F. *Phil. Trans. R. Soc. Lond. A* **273,** 547–581 (1973).
11. Jackson, M. J. in *Reefs, Canada and Adjacent Areas* (eds Geldsetzer, H. H. J., James, N. P. & Tebbutt, G. E.) 64–71 (Can. Soc. Petroleum Geologists, Calgary, 1989).
12. Press, W. H., Flannery, B. P., Vetterling, W. T. & Teukolsky, S. A. *Numerical Recipes in C: The Art of Scientific Computing* (Cambridge Univ. Press, New York, 1994).
13. Turcotte, D. L. *Fractals and Chaos in Geology and Geophysics* (Cambridge Univ. Press, 1992).
14. Kardar, M., Parisi, G. & Zhang, Y. *Phys. Rev. Lett.* **56,** 456–472 (1986).
15. Kim, J. M. & Kosterlitz, J. M. *Phys. Rev. Lett.* **62,** 2289–2292 (1989).
16. Amar, J. G. & Family, F. *Phys. Rev. A* **41,** 3399–3402 (1990).
17. Barabasi, A. L. & Stanley, H. E. *Fractal Concepts in Surface Growth* (Cambridge Univ. Press, 1995).
18. Edwards, S. & Wilkinson, D. *Proc. R. Soc. Lond. A* **381,** 17–31 (1982).
19. Grotzinger, J. P. & Read, J. F. *Geology* **11,** 710–713 (1983).
20. Hofmann, H. J. & Jackson, G. D. *Sedimentology* **34,** 963–971 (1988).
21. Sami, T. T. & James, N. P. *J. Sed. Res.* (in the press).
22. Sumner, D. Y. *Palaois* (submitted).
23. Knoll, A. H., Grotzinger, J. P. & Sergeev, V. *Geol. Soc. Am. Abstr. Progm.* A357 (1993).

ACKNOWLEDGEMENTS. We thank S. McGinnis for technical assistance in the early stages of this work, and I. Fairchild, B. Ginsburg, K. Grey, H. Hofmann, B. Runnegar and M. Walter for reviews of the manuscript. This work was supported in part by the US NSF and NASA.

CORRESPONDENCE should be addressed to J.P.G. (e-mail: grotz@grabau.mit.edu).

Evidence for a sound movement area in the human cerebral cortex

Timothy D. Griffiths*†‡, Adrian Rees*, Caroline Witton*, Ra'ad A. Shakir§, G. Bruce Henning‖ & Gary G. R. Green*

Departments of * Physiological Sciences and † Clinical Neuroscience, Newcastle University Medical School, Newcastle upon Tyne NE2 4HH, UK
‡ Wellcome Department of Cognitive Neurology, Institute of Neurology, 12 Queen Square, London WC1N 3BG, UK
§ Regional Neurosciences Centre, Charing Cross Hospital, Fulham Palace Road, London W6 8RF, UK
‖ Department of Experimental Psychology, Oxford University, South Parks Road, Oxford OX1 3UD, UK

HUMAN listeners can localize sounds by the difference in both arrival time (phase) and loudness between the two ears[1]. Movement of the sound source modulates these cues, and responses to moving sounds have been detected in animals in primary auditory cortex[2,3] and in humans in other cortical areas[4]. Here we show that detection of changes in the interaural phase or amplitude difference occurs through a mechanism distinct from that used to detect changes in one ear alone. Moreover, a patient with a right hemisphere stroke is unable to detect sound movement, regardless of whether it is defined by phase or by loudness cues. We propose that this deficit reflects damage to a distinct cortical area, outside the classical auditory areas, that is specialized for the detection of sound motion. The deficit is analagous to cerebral akinotopsia (motion blindness) in the visual system, and so the auditory system may, like the visual system[5], show localization of specialized functions to different cortical regions.

Detection of a sound movement from phase cues was investigated in control subjects by using a binaurally presented tone of 500 Hz in which the phase was sinusoidally modulated at 2 Hz. In one condition, as the phase was advanced at one ear, it was retarded at the other. This produces a changing delay between the waveforms at the ears, or interaural phase modulation (IPM), like that produced by a sound source oscillating in a horizontal arc around the head. Apart from changes in the interaural phase between the ears, this stimulus also modulates the instantaneous phase or frequency at either ear alone; a control stimulus was therefore used in which these frequency changes were identical at the two ears (binaural frequency modulation, FM). The interaural phase difference of the FM stimulus was always zero.

The detection of frequency- and phase-modulated stimuli is shown in Fig. 1*a*, *c* for six control subjects. The mean threshold (expressed as modulation index) was 1.24 for the detection of FM, and 0.313 for IPM. The IPM threshold for controls corresponds to a maximum interaural phase delay of 36 deg and, for an environmental sound, an average angular velocity of 85 deg s^{-1}. The data for naive subjects shows inter-subject variation, but the FM threshold for individual subjects exceeds the IPM threshold 4.7-fold (95% confidence interval, 2.8–6.8). Thus control subjects find it easier to detect a phase modulation at the two ears associated with the lateral movement of a sound source than to detect the associated frequency modulation. Together with the subjects' reports of a clear difference in the percept at threshold, this shows that the detection mechanism for IPM is distinct from those previously described for FM at low modulation rates[6,7]. At higher modulation rates, above 10 Hz, the detection of IPM and FM is similar for all subjects, and the perception of sound movement is lost.

Detection of sound movement from amplitude cues was also investigated in control subjects by using a binaurally presented tone sinusoidally amplitude modulated at 2 Hz. Analogous to the case with phase modulation, the stimuli had amplitude changes